Unifying energetic disorder from charge transport and band bending in organic semiconductors

Unifying Energetic Disorder from Charge Transport and Band Bending in Organic Semiconductors

Akchheta Karki, Gert-Jan A. H. Wetzelaer, Gollapalli Narayana Manjunatha Reddy, Vojtech Nadazdy, Martin Seifrid, Franz Schauer, Guillermo C. Bazan, Bradley F. Chmelka, Paul W. M. Blom, and Thuc-Quyen Nguyen*

Karki, M. Seifrid, Prof. G. C. Bazan, Prof. T.-Q. Nguyen Center for Polymers and Organic Solids University of California Santa Barbara (UCSB) Santa Barbara, CA 93106, USA E-mail: quyen@chem.ucsb.edu
Dr. G.-J. A. H. Wetzelaer, Prof. P. W. M. Blom Max Planck Institute for Polymer Research Ackermannweg 10, 55128 Mainz, Germany Dr. G. N. M. Reddy
Prof. B. F. Chmelka Department of Chemical Engineering University of California Santa Barbara (UCSB) Santa Barbara, CA 93106, USA Dr. V. Nadazdy Institute ofPhysics SAS Dubravsk a cesta 9, 845 11 Bratislava, Slovak Republic Prof. F. Schauer Tomas Bata University in Zlin Nad Stranemi 4511, Zlin CZ-760 05, Czech Republic

Keywords band bending, characterization techniques, charge transport, crystallinity, density-of-state widths, energetic disorder, organic conjugated polymers, solid-state NMR

Characterizing the density of states (DOS) width accurately is critical in understanding the charge-transport properties of organic semiconducting materials as broader DOS distributions lead to an inferior transport. From a morphological standpoint, the relative densities of ordered and disordered regions are known to affect charge-transport properties in films; however, a comparison between molecular structures showing quantifiable ordered and disordered regions at an atomic level and its impact on DOS widths and charge-transport properties has yet to be made. In this work, for the first time, the DOS distribution widths of two model conjugated polymer systems are characterized using three different techniques. A quantitative correlation between energetic disorder from band-bending measurements and charge transport is established, providing direct experimental evidence that charge- carrier mobility in disordered materials is compromised due to the relaxation of carriers into the tail states of the DOS. Distinction and quantification of ordered and disordered regions of thin films at an atomic level is achieved using solid-state NMR spectroscopy. An ability to compare solid-state film morphologies of organic semiconducting polymers to energetic disorder, and in turn charge transport, can provide useful guidelines for applications of organic conjugated polymers in pertinent devices.

1. Introduction

An accurate depiction of the electronic structures of organic semiconducting polymers can have important implications in understanding their performances when incorporated in organic solar cells, [1] organic field-effect transistors (OFETs),[2] and organic light-emitting diodes (OLEDs).[3] Unlike ordered crystalline semiconductors such as silicon, which have clearly defined conduction and valence bands, disordered organic systems such as polymeric semiconductors have a broadened electronic density-of-states (DOS) distribution.[4] This broadening is a result of the different types of intra- and intermolecular interactions, rotation and kinking of polymer chains, and conformational diversity that gives rise to a morphologically diverse film.[5] The DOS distribution is frequently described by a Gaussian function, where the extent of broadening is determined by the variance sigma (a). A consequence of a broadened DOS is that low-energy tail states extend far into the

bandgap, which give rise to thermally activated hopping transport. In fact, different experimental and theoretical studies have characterized these tail states in organic semiconductors, revealing either Gaussian or exponential shaped tails.[6-23] Characterizing energetic disorder accurately is important in understanding the charge-transport properties of organic polymer semiconductors as broader DOS distributions generally give rise to an inferior transport. In turn, the performance of organic semiconductor devices largely depends on the charge-transport properties of the organic semiconductor.![24-29]! From a morphological standpoint, the relative densities of ordered and disordered regions in thin films are known to affect charge-transport properties with crystalline regions enhancing charge transport due to the high degree of n-n stacking of backbone moieties and lamellar structural order of sidechains.[30-31] However, to this end, a comparative study between molecular structures showing clearly distinguishable ordered and disordered regions at an atomic level and its impact on the DOS widths and ultimately the charge-transport properties have yet to be established.

Additionally, while there exist several techniques in the literature that give relevant information on the shape or width of the DOS distribution, efforts to try and unify these different techniques are lacking. In this work, we characterize the DOS distribution widths of two structurally unique organic semiconducting polymers using temperature-dependent current density- voltage J-V) measurements, Kelvin probe measurement (KP) of band bending, and energy-resolved electrochemical impedance spectroscopy (ER-EIS). In order to eliminate unexpected changes in morphology due to additional post-processing steps, both polymers were dissolved in the same solvent (chlorobenzene), and spincoated for all characterization techniques. From a comparison of the DOS widths measured using these three techniques to a parallel measurement of charge transport, we establish a quantitative relationship between charge transport and band-bending measurements for the first time. For a standardized and comparative study incorporating all three techniques, two conjugated polymers **(Figure 1)**, poly[4,8-bis(5-(2-ethylhexyl)thiophen-2-yl) benzo[1,2-b;4,5-b']dithiophene-2,6-diyl-alt-(4-(2-ethylhexyl)-3- fluorothieno[3,4-b]thiophene-)-2-carboxylate-2-6-diyl)] (PTB7-Th) and poly [2-methoxy-5 - (2 -ethylhexyloxy) -1,4-phenylenevinylene] (MEH-PPV) were selected with clearly distinct charge-transport properties. MEH-PPV is a conjugated polymer commonly used in OLEDs and PTB7-Th is a conjugated polymer commonly used as a donor material in organic bulk heterojunction solar cells.

2. Results and Discussion

2.1. Temperature-Dependent Mobility Measurements for Characterizing Charge Transport and Energetic Disorder

To characterize hole transport and energetic disorder of transport sites in these polymers using *J-V* measurements, symmetric hole-only devices were fabricated. Films of the pristine polymers were sandwiched between an indium tin oxide (ITO)/PEDOT:PSS (35 nm) bottom contact and an MoO_3 layer (10 nm) capped with Ag (100 nm) top contact. A previous study has shown that the work functions of PEDOT:PSS (=5.2 eV) and MoO_3 (=6.9 eV[32]) are sufficient to act as Ohmic hole- injecting contacts into the MEH-PPV HOMO level of =-5.3 eV and produce symmetric *J-V* curves[33]; this is also shown to be the case for the PTB7-Th polymer in this study, which has an HOMO of =-5.2 eV (see **Figure S1**, Supporting Information).[34]

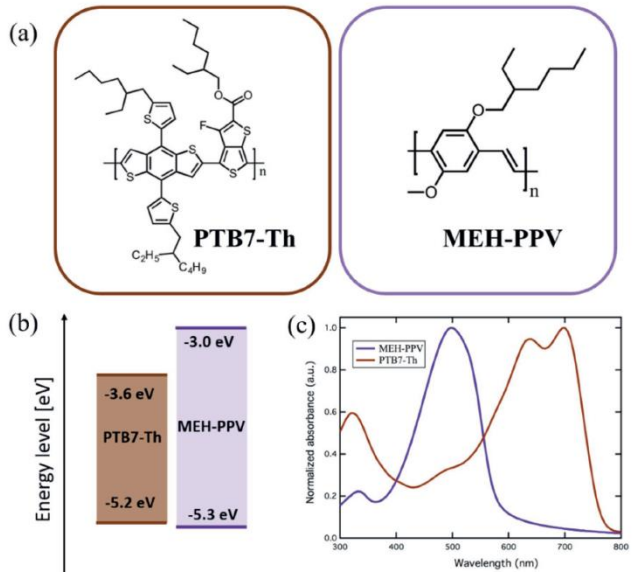

Figure 1. a) Chemical structures of PTB7-Th and MEH-PPV. b) Energy levels showing highest occupied molecular orbital (HOMO) and lowest unoccupied molecular orbital (LUMO) levels of the two polymers. c) Normalized absorption spectra of the polymers.

Measurement of space-charge-limited currents (SCLC) is a widely established method to characterize charge transport in conjugated polymers.[35_36] The expression for an SCLC in a diode sandwiched between two metal contacts derived by Mott and Gurney is where, $\varepsilon_0$is

$$J = \frac{9\varepsilon_0 \varepsilon_r \mu V^2}{8L^3} \qquad (1)$$

the vacuum permittivity, *£,.* is the relative permittivity of the material, μ is the charge-carrier mobility, and *L* is the active layer thickness. In order to determine the mobility from experimental data, it should first be verified that the measured currents are indeed limited by space charge.

The experimentally measured *J-V* characteristics of PTB7-Th **(Figure 2a)** and MEH-PPV **(Figure 2c)** hole-only devices on a double logarithmic scale show Ohmic currents at low voltages and a transition to a quadratic voltage dependence at higher voltages. The quadratic voltage dependence is characteristic of SCLC, with the Ohmic current at low voltage being due to the diffusion contribution to the current, which is neglected in the derivation of equation (1). As established from equation (1), a pre-requisite for satisfying the criterion for SCLCs in a diode is that the current has an L^{-3} dependence on the thickness of the diodes. As shown in **Figure 2b, d**, when multiplying the current density by L^3 the current densities almost coalesce— now with little deviation between the highest current density (thinnest) and the lowest current density (thickest) device— confirming that the thickness dependence behavior expected for SCLCs is indeed satisfied. The thickness dependence is slightly stronger than L^{-3}, which is due to the density dependence of the mobility.[33] Fits to equation (1) shown by the black dotted lines in Figure 2b,d give average mobilities of 2.7 ± 0.7 x 10^{-3} cm^2 Vs^{-1} for PTB7-Th and 4.2 ± 2 x 10^{-5} cm^2 Vs^{-1} for MEH-PPV for the range of layer thicknesses.

A limitation of using equation (1) to extract the charge- carrier mobility is that while it describes the experimental data well in low electric field regimes and at room temperature, it fails to describe the current density-voltage characteristics at higher fields—especially at lower temperatures. The reason for this discrepancy is the fact that the mobility is not constant, as assumed in equation (1) (see **Figure S2**, Supporting Information).

As a result of energetic disorder of hopping sites, the mobility in organic semiconductors is chargecarrier density, electric field, and temperature dependent.[37] In 2005, Pasveer et al. developed a model referred to as the extended Gaussian disorder model (EGDM) that describes the density, electric field, and temperature dependence of mobility in a system with localized states having a Gaussian distribution of energy.[38] The parameters describing transport in the EGDM are the width of the DOS distribution (σ), the lattice constant (a), and a mobility pre-factor (μ∞j. The temperaturedependent mobility at zero field and density is given by

$$\mu_0\ (T) = \mu_\infty\ c_1 \exp\left[-c_2 \left(\frac{\sigma}{kT}\right)^2\right] \qquad (2)$$

where, c_1 = 1.8 x 10^{-9} and c_2 = 0.42 are constants derived from the EGDM,[38] *k* is the Boltzmann constant, and *T* is the temperature. The temperature dependence of mobility is exclusively determined by the energetic disorder *a* which enables us to extract the energetic disorder from the temperature dependence of mobility. We have incorporated the EGDM mobility function in a drift-diffusion model[39] to simulate the full current density-voltage characteristics.

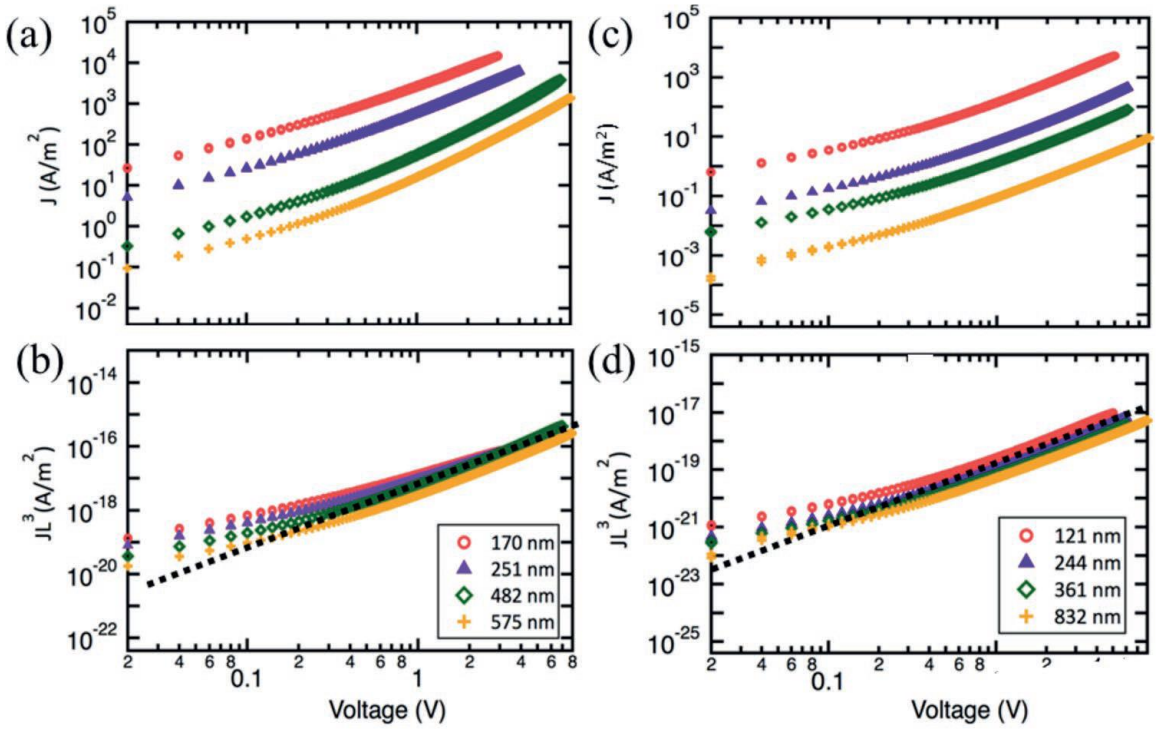

Figure 2. *J-V* characteristics of symmetric a) PTB7-Th and c) MEH-PPV diodes of different layer thicknesses at 300 K. The current density is multiplied by L^3 for b) PTB7-Th and d) MEH-PPV to show the layer-thickness dependence of current. The dotted black lines on Figure 2b, d represent the average fits to equation (1) for different thicknesses.

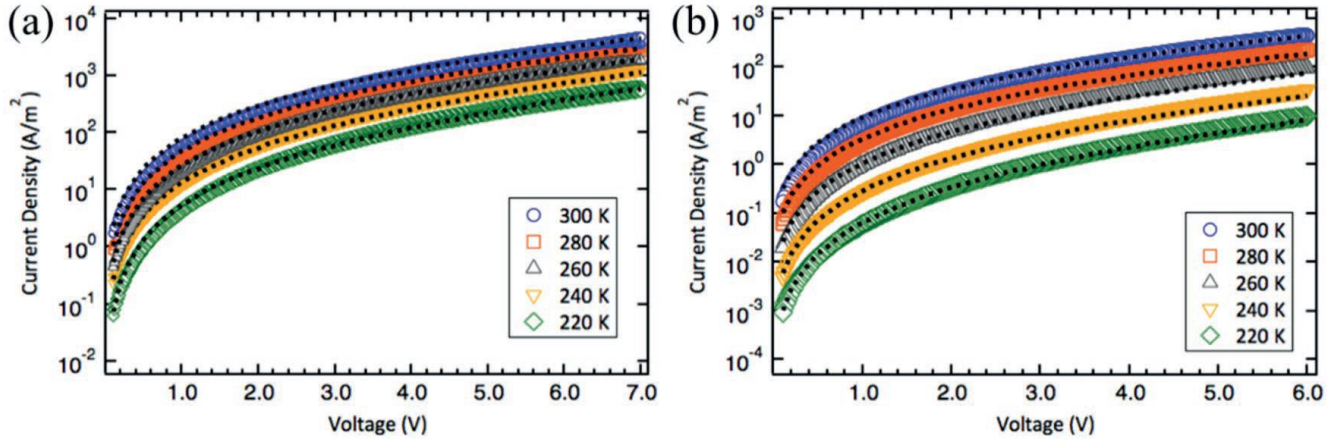

Figure 3. Temperature-dependent *J-V* characteristics of a) PTB7-Th and b) MEH-PPV hole-only diodes with a layer thickness of 481 and 244 nm, respectively. Dotted lines correspond to calculations obtained from a drift-diffusion model.

Figure 3a, b shows the experimental temperature-dependent *J-V* curves for PTB7-Th and MEH-PPV in the forward bias along with the simulations (dotted lines) obtained from a numerical drift-diffusion model, which now takes the charge- carrier density, electric field, and temperature dependence into account, according to the EGDM. For PTB7-Th, best fits were obtained using σ = 75 meV and a = 4.5 nm. This set of parameters was found to be consistent across devices with different layer thicknesses (see Figure S3, Supporting Information). The fits to the experimental data for three different layer thicknesses gave a mobility of 1.6 x 10^{-3} cm^2 Vs^{-1} at vanishing charge-carrier densities and electric field at room temperature. This mobility is slightly lower than the mobility obtained from fits to equation (1) shown in Figure 2b,d and relatively high for a bulk value, which is consistent with weak temperature dependence[22] and a small value for the energetic disorder.

It is visually apparent that the MEH-PPV *J-V* curves have a stronger temperature dependence than PTB7-Th, indicating a stronger temperature dependence of the mobility. The *J-V* characteristics were fitted with the drift-diffusion model using σ = 125 meV and a = 2.2 nm. Also, in this case, this set of parameters was found to be consistent across all layer thicknesses (see Figure S5, Supporting Information) and fits to all the experimental data gave a room-temperature mobility of 5.9 x 10^{-6} cm^2 Vs^{-1} at vanishing charge-carrier densities and electric field. The lower value of a for MEH- PPV is consistent with its disordered and amorphous nature in comparison to the highly crystalline PTB7-Th film. The lower mobilities obtained at vanishing charge-carrier densities and electric field compared to mobilities from the SCLC fits (Figure 2b,d) confirm the density and electric-field dependence of mobility—which is more pronounced in the more disordered MEH-PPV polymer. The higher energetic disorder for MEH-PPV is consistent with its lower charge-carrier mobility.

It is worth noting the slightly lower σ and higher n for MEH- PPV reported in this study from that reported in literature[133,401] is likely due to the difference in the M_w of MEH-PPV used (1000 000 Da[,33,40]] versus 125 000 Da in this study). This discrepancy alludes to the fact that the molecular weight *(M_w)* of polymers can play a rather significant role in the orientation of polymer chains in a film, thereby giving rise to the observed differences in the energetic disorder term, σ, as well as the charge-carrier mobility, μ.[41,421

2.2. Kelvin Probe Method for Characterizing Tail States Disorder

The width of the Gaussian DOS distribution obtained from the charge-transport measurements was determined to be 75 meV for PTB7-Th and 125 meV for MEH-PPV. We now compare these values to the DOS distribution widths obtained by a second technique, where a KP is used to measure band

bending in the conjugated-polymer films. KP is a capacitive, non-contact measurement that measures the contact potential difference (CPD) between a tip and a semiconductor film of interest, deposited on a conductive substrate. The CPD gives the Fermi energy at the surface of the semiconductor with respect to a calibrated tip.[43,44]

One of the first ever studies of band bending of conjugated polymer layers was done by Blakesley and Greenham.[1451] When a semiconductor is in contact with an electrode with a high or low work function, such that an Ohmic contact is formed, the semiconductor exhibits band bending in the vicinity of the electrode due to the charge transfer to establish thermodynamic equilibrium across the interface. The high carrier density at the interface results in a gradient in the electrostatic potential, giving rise to a diffusion of carriers, accompanied by band bending.[145,461] It has been shown that the amount of bending is a function of energetic disorder, with a broader DOS distribution resulting in more band bending. The KP technique can probe this gradient in electrostatic potential, which allows for extraction of the width of the DOS distribution.

An expression for the distribution of charge carriers *(n(x))* diffusing in from the electrode into the polymer semiconductor and the subsequent change in the electrostatic potential *(V(x))* in the film can be found by solving an expression for the charge-carrier density *(n)* from a certain distance (x) of the polymer-electrode interface using a combined expression of the Fermi-Dirac distribution and the DOS of the polymer, as shown in equation (3) below

$$n(x) = \int_{-\infty}^{\infty} \frac{1}{1+\exp[(E-E_F)/k_BT]} g[E+eV(x)]dE \qquad (3)$$

where *E* is energy, k_B is the Boltzmann constant, *T* is temperature, *g(E)* is the model DOS, and *V(x)* is the electrostatic potential. *V(x)* is obtained by solving the 1D Poisson's equation (4) below

$$\frac{d^2V}{dx^2} = \frac{en(x)}{\varepsilon} \qquad (4)$$

with the assumption that the electric field vanishes at the polymer surface, ε is the elementary charge, and *e* is the permittivity of the polymer film.[1461] Equation (5) is the Gaussian DOS function that was used to fit the data.

$$g(E) = \frac{N_0}{\sigma\sqrt{2\pi}} \exp\left[-\frac{(E-E_0)^2}{2\sigma^2}\right] \qquad (5)$$

Here, N_0 is the integrated state density, *a* is the width of the Gaussian DOS, and E_0 is the center of the distribution. The Gaussian DOS model can only be solved numerically by varying E_0 and *a* to obtain the best fit to the experimental data. For an exponential DOS distribution, on the other hand, an analytical model was expressed as a function of the film thickness, d.[46-47]

$$d = \sqrt{\frac{2E_t\varepsilon_0\varepsilon_r}{q^2N}} \exp\left(\frac{|\varphi(d)|}{2E_t}\right) \arccos\left[\exp\left(-\frac{|\varphi(d)|}{2E_t}\right)\right] \qquad (6)$$

In equation (6), *d* is the film thickness, E_t is the exponential disorder term of the DOS, *e* is the relative dielectric constant, e_o is the vacuum permittivity, *N* is the DOS maximum, and *q(d)* is the net potential shift at a distance *d* from the electrode.

Figure 4 shows the band-bending fits for a Gaussian and exponential DOS distribution to the experimentally measured work function values at different layer thicknesses for the two polymers. Both polymers were spin coated on top of the high work function electrode MoO_3, to ensure diffusion of holes from the electrode into the HOMO of the organic semiconducting polymer, giving rise to band bending. The Gaussian and exponential models describe the DOS function in characteristically different ways with the Gaussian DOS tailing off faster as a function of site energy than the exponential DOS.[1481]

The band-bending method is only sensitive to the tail states and it is not possible to distinguish a preference between the two models from this analysis. Therefore, fits to the experimental band-bending profiles can give estimates for both disorder parameters—a for the Gaussian model and E_t for the exponential model.

As shown in Figure 4a, in the case of PTB7-Th, there is minimal change in the work function of the film with increasing thickness. This is equivalent to a small degree of band bending. A fit to equation (6) gives an exponential disorder (E_t) term of 26 meV—which is almost equivalent to kT and is the limit for the application of the exponential DOS model. The disorder width (a) obtained from the Gaussian DOS model is 7o meV. Furthermore, previous reports have shown that band-bending profiles that show a quick, sharp plateau at relatively small (<10 nm) thicknesses—which is the case for PTB7-Th—is indicative of highly ordered films.[46-49,50] On the other hand, the band-bending profile for MEH-PPV (Figure 4b) shows a larger change in the work function of films with increasing polymer thickness. Both exponential DOS and Gaussian DOS fits to the band-bending profiles for this polymer reveal large DOS widths, giving E_t of 52 meV and a of 130 meV, respectively.

2.3. Energy-Resolved Electrochemical Impedance Spectroscopy (6) Method for Characterizing Tail States Disorder

Using the KP method, we obtain exponential DOS widths of 52 and 26 meV for MEH-PPV and PTB7-Th, respectively. These values are now compared to the exponential widths of the DOS distributions from a third technique, namely ER-EIS. There has been significant progress in the last few decades on EIS methods.[1511] Recently, a novel ER-EIS method was developed as a way to measure the DOS of organic polymers over wide energy ranges.[152-531] The ER-EIS technique is based on the reduction-oxidation reaction occurring at the interface of a polymer semiconductor film and an electrolyte. In the experimental set-up, an electrochemical cell is placed on a conductive ITO substrate spin-coated with an organic polymer semiconductor film. The DOS of an organic polymer film can be measured by sweeping an externally applied potential (U) of the polymer thin film in order to modify the Fermi level. At each applied potential, U, impedance spectroscopy is performed by applying a small perturbing potential at different frequencies.

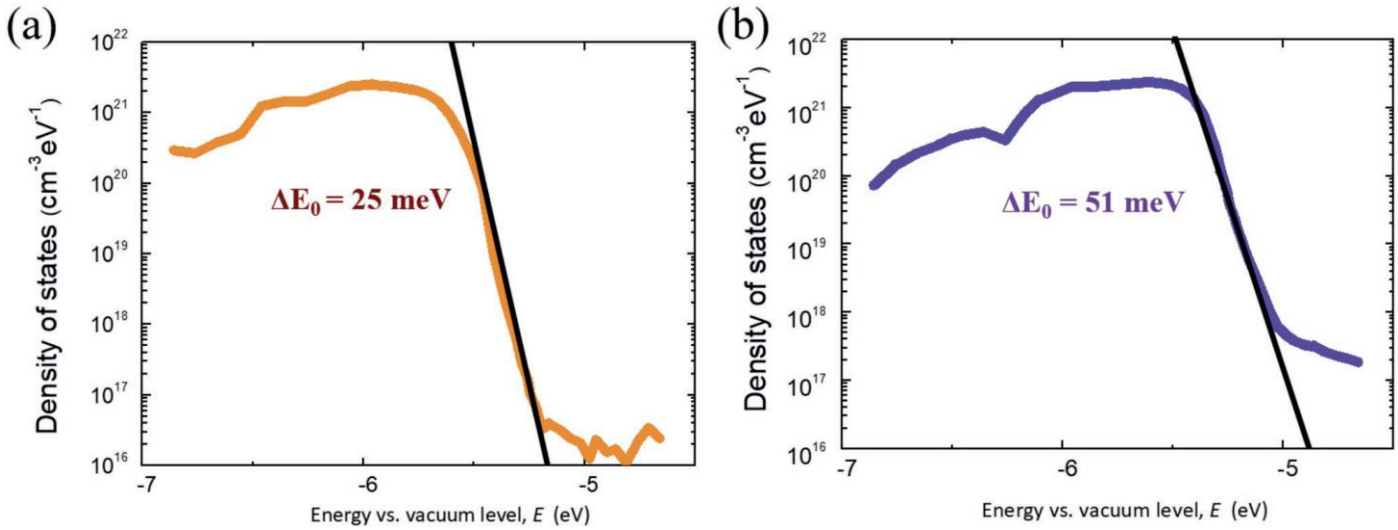

Figure 4. Band-bending profiles of a) PTB7-Th and b) MEH-PPV films cast on 70 nm thick M0O3 layer.

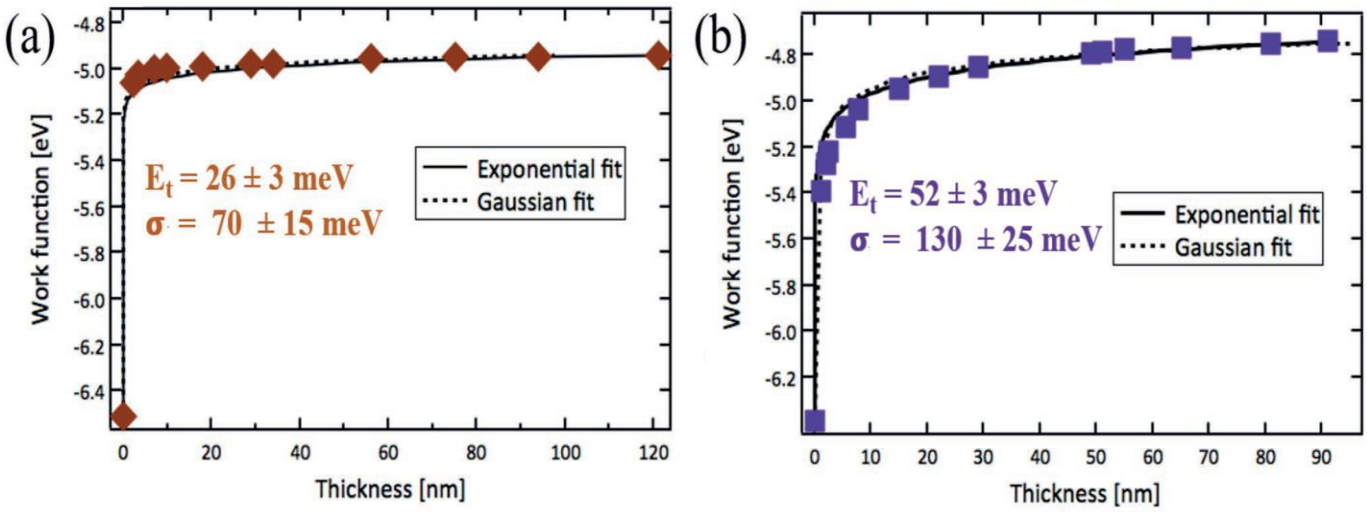

Figure 5. HOMO DOS functions of a) PTB7-Th and b) MEH-PPV films measured by the ER-EIS method

A few assumptions are made in order to derive the DOS from the measured redox current at the semiconductor-electrolyte interface.[1521] The charge-transfer current density between the electrolyte and the semiconductor surface can be written as

$$j = ek_{et}n_s[A] \qquad (7)$$

where e is the elementary charge, k_{et} is the chargetransfer coefficient, n_s is the semiconductor surface carrier concentration at the Fermi level, and $[A]$ is the electrolyte concentration.

In order to construct the DOS from the ER-EIS method, it is defined as the number of states at a given energy E in an energy interval dE, such that $g(E) = dn/dE$. With the assumption that the surface electronic structure of the polymers is well represented by that of the bulk, the DOS can now be written in the form below

$$g\left(E_F = eU\right) = \frac{dn_s}{d(eU)} \qquad (8)$$

Since the application of the perturbing potential varies n_s, the charge-transfer resistance can be found experimentally, where $R_{ct} = dU/d(jS)$.

Substituting equation (7) to equation (8), and replacing the expression for R_{ct}, the DOS function at the Fermi energy, $g(E_F)$, can now be expressed in terms of the charge-transfer resistance, R_{ct}, under an applied voltage U, as follows:

$$g\left(E_F = eU\right) = \frac{1}{e^2 k_a [A] S R_{ct}} \qquad (9)$$

where, S is the active sample surface area. From equation (9), the reconstructed DOS, $g(E_F)$, is found to be inversely proportional to the experimentally measured charge-transfer resistance term, R_{ct}.[52]

Figure 5 shows the ER-EIS measurements of the electronic structures of the polymers. In contrast to other competing methods,[17,8,54-561] information about the DOS parameters can be directly obtained from the measured spectra by using ER-EIS. By fitting the extremities of the HOMO DOS with an exponential dependence, the exponential disorder parameter ΔE_0 can be found, which corresponds to the exponential disorder arising from the tail states of the HOMO DOS distribution. In this analysis, a steeper slope obtained from the exponential fit corresponds to a narrower DOS width. The exponential disorder terms obtained from fitting the DOS extremities using this method is 25 meV for PTB7-Th and 51 meV for MEH-PPV.

2.4. Connecting the DO(T)S: Unification of Charge Transport and Band Bending

The energetic disorder terms for the HOMO DOS from the Gaussian and exponential models using different techniques are summarized in **Table 1**. A measure of disorder using these different techniques give agreeable estimates of disorder values. A good agreement is found between the Gaussian widths estimated using the KP and temperature-dependent *J-V* measurements—with values for both polymers falling within error of each other. The exponential widths estimated from KP and ER-EIS methods are also in agreement. It is worth noting that the correlation observed between the Gaussian and exponential DOS width values obtained from this work for both polymers is equivalent to the correlation reported in the literature.[37]

Table 1. Comparison of Gaussian and exponential energetic disorder terms obtained from Kelvin probe, temperature-dependent*J-Vs* (EGDM), and ER-EIS methods.

Donor polymer	σ_t (Kelvin probe) [meV][a)]	σ_o (Temperature-dependent *J–V*) [meV][a)]	E_t (Kelvin probe) [meV][a)]	ΔE_0 (ER-EIS) [meV][a)]
MEH-PPV	130 ± 25	125 ± 10	52 ± 3	51
PTB7-Th	70 ± 15	75 ± 10	26 ± 3	25

[a)]Measurements for each technique were repeated three times for reproducibility.

The similar values obtained from the different techniques can be attributed to the common assumptions and conditions in each measurement. Discrepancies in mobility values between holeonly diodes and field-effect transistors have been shown to be due to differences in the values

of charge-carrier densities at operating conditions (10^{21}-10^{23} m^{-3} for diodes versus 10^{23}-10^{25} m^{-3} for FETs).[37] The similar DOS widths obtained from all three techniques in this study can likely be attributed to the similarities in charge-carrier densities in all three techniques (10^{21}-10^{23} m^{-3}).[33,49,52]

KP and ER-EIS techniques are both based on the band-bending phenomenon happening at a semiconductor- electrode or semiconductor-electrolyte interface, which is independent of any influence of electric field or light intensity. While temperature-dependent *J-V* measurements are done under the influence of an applied electric field and at different temperatures, the EGDM model takes the electric field, charge-carrier density, and temperature dependence into account, thereby bearing out a disorder value that has no influence on such extrinsic effects. While KP and ER-EIS techniques specifically probe only the tail states of the DOS distribution, EGDM assumes that the whole DOS distribution is described by a single Gaussian. An important assumption in obtaining the DOS width is that charge carriers be under no influence of applied electric field or light intensity, and so the assumptions during the measurements (from KP and ER-EIS) and in the analysis for the EGDM (from *J-V* measurements) ensure that in the DOS width being probed, the effect of charges near the tail states of the DOS distribution— where the number of charge carriers are much less than the number of hopping sites—are taken into account

2.5. Quantification of Ordered and Disordered Regions in Thin Films Using GIWAXS and Solid-State NMR

For a better understanding of the origins in the differences of charge transport and DOS widths between these two structurally distinct polymers, we complement the experimentally measured energetic disorder values with a suitable study of the solid-state film morphology. It has long been established that degrees of film crystallinity play crucial roles in determining the charge-transport properties; specifically, more crystalline films lead to higher charge-carrier mobilities![57-59] GrazingIncidence Wide-Angle X-Ray Scattering (GIWAXS) is a commonly used technique to probe the relative differences in the long-range order of films. Qualitative comparison of the 100 reflections in the GIWAXS patterns of PTB7-Th and MEH-PPV films (Figure S4, Supporting Information) showed MEH-PPV with a broader peak indicative of more features that are randomly oriented in this film in comparison to the narrower reflection pattern of PTB7-Th.[60] Furthermore, the crystalline coherence length *(L_c),* which is a quantity related to the average crystal size in a film, is larger for PTB7-Th in both the in-plane and out-of-plane directions (Table S1, Supporting Information).[60] A drawback to GIWAXS, however, is that it only detects signals coming from the crystalline contents in a film and so, accurately quantifying the absolute amount of crystalline and amorphous regions in a film requires the use of additional complementary techniques![61]

For the purpose of identifying and quantifying the ordered and disordered backbone regions in the spin-coated PTB7-Th and MEH-PPV thin films, solid-state magic-angle-spinning (MAS) NMR was used to probe the structures of these polymers at a molecular level. Solid-state MAS NMR is sensitive to local (ca. 1 nm) bonding environments and complements scattering analyses that are sensitive to longrange structural order (ca. 100s nm).[62-65] Specifically, ^{1}H, ^{13}C, and ^{19}F isotropic chemical shifts provide information on backbone conformation and inter- or intramolecular interactions. In this respect, the presence of well-ordered backbone moieties is expected to yield relatively narrow ^{1}H and ^{19}F signals, whereas disordered regions exhibit relatively broad signals that manifest distributions of polymer conformations and structural disorder associated with the backbone moieties. In addition, the ordered and disordered regions of alkyl sidechains can be distinguished on the basis of the y-gauche effect[66]; for example, when two -CH_2- groups are in a /-position relative to one another and in *trans/trans* (tt) configurations, the isotropic ^{13}C chemical shifts are displaced to higher frequencies, compared to the same moieties with *trans/gauche (tg)* or *gauche/gauche* (gg) conformations that are displaced to lower frequencies. Analyses of ^{1}H, ^{13}C, and ^{19}F NMR isotropic

chemical shifts and integrated signal intensities are therefore expected to provide quantitative information on the relative populations of different polymer moieties in ordered and disordered regions, which is difficult to obtain from X-ray scattering and electron microscopy techniques.

Analyses of 1D solid-state ^{1}H MAS NMR spectra of PTB7-Th and MEH-PPV enabled numerous ^{4}H signals associated with polymer backbone and sidechain moieties to be identified and distinguished (Figure S5, Supporting Information), but not all, as severely overlapped signals stemming from 17 chemically distinct ^{4}H sites in PTB7-Th and 10 different ^{4}H sites in MEH- PPV hinder the assignment of these ^{4}H signals. The ^{4}H signals from the PTB7-Th sidechains are only partially resolved due to structurally identical sidechains substituted on the thiophene and thienothiophene moieties in comparison to the analogous ^{4}H signals from the MEH-PPV sidechains. Nevertheless, the high intrinsic sensitivity, high natural abundance (100%), and substantial chemical shift range associated with ^{19}F MAS NMR permitted ^{19}F signals to be resolved and assigned to specific fluorine atom moieties, on which the quantitative description of ordered and disordered backbone regions in PTB7-Th is based. The 1D ^{19}F MAS NMR spectrum of PTB7-Th powdered thin films acquired at 30 kHz MAS (**Figure 6**a) showed a narrow signal at -110 ppm that corresponds to ^{19}F sites in ordered PTB7-Th backbone moieties, along with broad weak signals in the ranges -125 to -135 ppm and -155 to -170 ppm, which were attributed to fluorine atoms in disordered PTB7- Th backbone moieties. Integration of the ^{19}F signal intensities indicates that the vast majority (99 ± 1%) of the ^{19}F atoms are in locally ordered PTB7-Th backbone environments (-110 ppm), with a very small percentage (<1%) in disordered backbones.

To distinguish between ordered and disordered regions in MEH-PPV thin films, a single-pulse ^{13}C MAS NMR spectrum was acquired and analyzed (Figure 6b). On the basis of isotropic ^{1}C chemical shifts of MEH-PPV reported in the literature'[67]' and subsequent line shape analyses, the ^{13}C signals in the aromatic region could be assigned to the backbone moieties, as follows: 151 ppm to carbon atoms *C1* and *C4,* 126 ppm to *C3* and C6, 120 ppm to *C7* and *C8,* and the range 107-112 ppm to *C2* and *C5.*

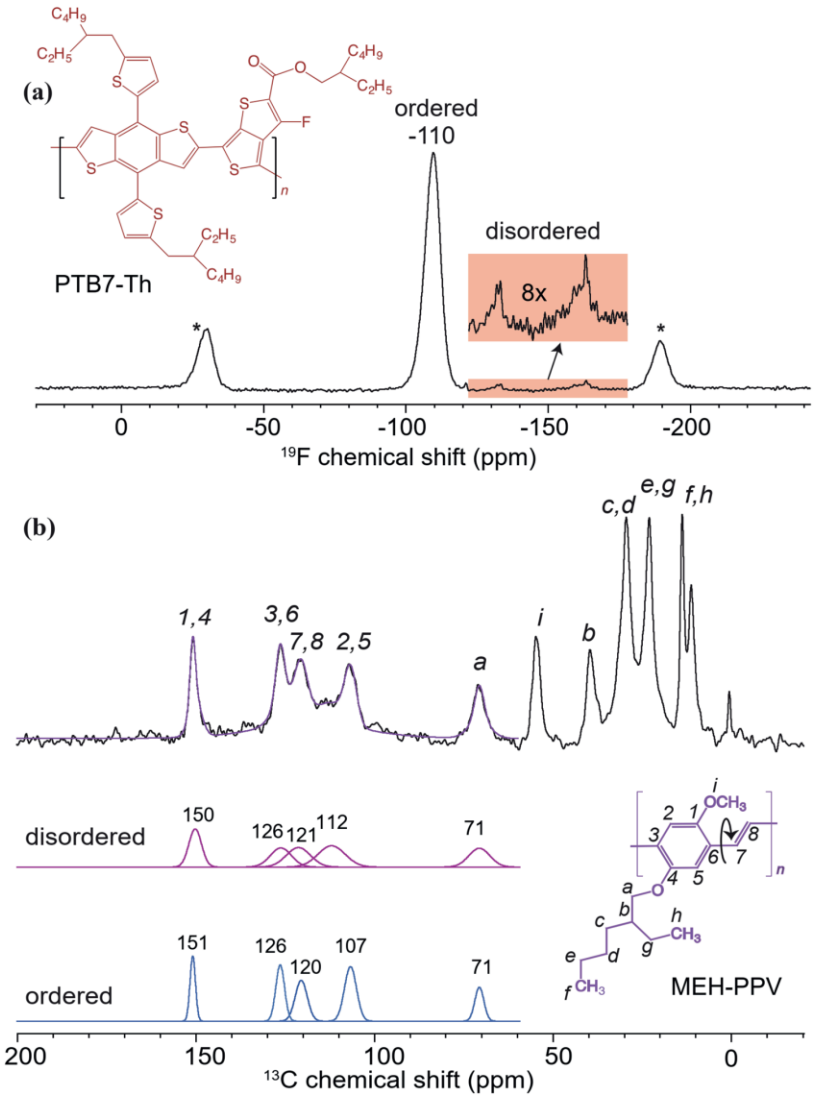

Figure 6. a) Solid-state 1D ^{19}F MAS NMR spectrum acquired at 9.4 T, 298 K, and 30 kHz MAS for powdered PTB7-Th films. b) Solid-state 1D ^{13}C MAS NMR spectrum of powdered MEH-PPV films acquired at 9.4 T, 298 K, and 15 kHz MAS. *correspond to spinning sidebands.

Similarly, in the alkyl region of the spectrum, the ^{13}C signals are assigned to the alkyl sidechains, as follows: 71 ppm to carbon atom *Ca,* 55 ppm to *Ci,* 40 ppm *Cb,* 30 ppm to *Cc* and *Cd,* 23 to *Ce* and *Cg,* 14 to *Cf,* and 11 ppm to *Cg.* In particular, the ^{13}C chemical shifts of carbon atoms *C2* and *C5* are expected to be sensitive to conformational differences across the *C5-C6-C7-C8* dihedral angle that bisects the phenylene and vinylene moieties: the narrow ^{13}C signal at 107 ppm is attributed to *C2* and *C5* atoms in ordered MEH-PPV backbones and the broad ^{13}C intensity centered at 112 ppm is attributed to *C2* and *C5* atoms in disordered MEH-PPV backbones.[68] Line shape analyses of partially resolved signals were deconvoluted to estimate the relative fractions of ordered and disordered regions of MEH-PPV backbones. The average of integrals of the deconvoluted ^{13}C signals associated with the *C1-C8* moieties indicate that the MEH-PPV film consisted of 43 ± 5% ordered and 57 ± 5% disordered backbone moieties, respectively. Thus, quantitative solid-state ^{19}F and ^{13}C NMR analyses suggest that PTB7-Th films have relatively higher fraction of ordered conjugated backbone regions, compared to the backbone moieties in the MEH-PPV films, which is consistent with the measured differences in the DOS widths and with their distinct charge- carrier properties.

3. Conclusion

To summarize, here for the first time by using three different techniques, a quantitative correlation between energetic disorder from band-bending measurements and charge transport is established.

This work provides direct experimental evidence that charge-carrier mobility is compromised due to the relaxation of carriers into the tail states of the DOS. An amorphous and disordered polymer, MEH-PPV, with a low charge-carrier mobility and a crystalline and ordered polymer, PTB7-Th, with a high charge-carrier mobility both show trap-free hole transport and reveal distinctly different energetic disorder values as a result of different film morphologies. By combining quantitative solid-state film morphology studies of organic semiconducting polymers at an atomic level to energetic disorder and in turn charge transport, this work presents useful guidelines to characterize organic semiconducting polymers for applications in pertinent devices

4. Experimental Section

Materials: Poly[4,8-bis (5-(2-ethyl hexyl) thiophen-2-yl)benzo[1,2-b;4,5- b']dithiophene-2,6-diyl-alt-(4-(2-ethylhexyl)-3-fluorothieno[3,4-b] thiophene-)-2-carboxylate-2-6-diyl)] (PTB7-Th) of M_w 145 000 Da and Poly[2-methoxy-5-(2-ethylhexyloxy)-1,4-phenylenevinylene] (MEH-PPV) of M_w 120 000 Da were purchased from one material and used as-received.

Hole-Only Diode Fabrication: Diodes were prepared on Corning glass substrates patterned with 140 nm of ITO and scrubbed with detergent followed by sonication in soapy water, deionized water, acetone, and isopropanol. Substrates were then treated with O_2 plasma for 30 min and spin-coated with a =35 nm thick poly(3,4-ethylenedioxythiophene): poly(styrenesulfonate) (PEDOT:PSS) (Clevios P VP Al 8043) layer and annealed in air for 20 min at 140 °C. Pristine polymer solutions in chlorobenzene were prepared inside the glovebox and left stirring on a hot-plate overnight before spin-coating the films onto the layer of PEDOT:PSS films inside a nitrogen-filled glovebox. In order to ensure an unchanged morphology for polymer films made with different thicknesses, the polymer solution concentrations were varied while keeping the spin speeds constant at 1500 rpm. The devices were finished with a deposition of a 10 nm MoO_3 layer followed by a 100 nm Ag capping layer with a thermal evaporator at a pressure of less than 1 x 10^{-6} Torr.

Electrical Measurements: Temperature-dependent*J-V*curves of diodes were measured using a liquid nitrogen cryostat with a Keithley 2602A system source-meter and a Lakeshore 321 temperature controller at a pressure of less than 1 x 10^{-6} Torr. Film thicknesses were measured using an Ambios XP-100 profilometer.

Kelvin Probe Measurements: Films of PTB7-Th and MEH-PPV were cast on ITO substrates with a 70 nm evaporated MoO_3 layer. The concentration of films cast on substrates were varied to obtain a range of layer thicknesses. All polymer films were spin cast at 1500 rpm to avoid any morphological changes. CPD values were measured using a SKP 5050 (KP technology, UK) KP with a stainless-steel tip of 2 mm diameter. The probe work function was calibrated against freshly cleaved highly ordered pyrolytic graphite (HOPG), with its work function assumed to be 4.6 eV.[69,70] All measurements were done inside an inert nitrogen-filled glovebox.

Energy-Resolved Electrochemical Impedance Spectroscopy: Electrochemical microcells were formed on ITO substrates with deposited polymer thin films. All polymer films were spin cast at 1500 rpm to avoid any morphological changes. The solution of 0.1 M TBAPF6 in anhydrous acetonitrile was used as the supporting electrolyte. The dissociation of this electrolyte in the inert atmosphere occurred at an overpotential of V. The active polymer electrode area was 12 mm^2. The potential of the working electrode with respect to the reference Ag/AgCl electrode was controlled via a potentiostat. Pt wire was used as the counter electrode. The potential recorded with respect to the reference Ag/AgCl electrode was recalculated to the local vacuum level assuming the Ag/ AgCl energy versus vacuum value of 4.66 eV. An Impedance/gain-phase analyzer, Solartron analytical, model 1260 (Ametek, Berwyn, USA), was used. The AC harmonic voltage signal frequency was 0.5 Hz, its amplitude was

100 mV, and the sweep rate of the DC voltage ramp was 10 mV s^{-1}. Bode and Cole-Cole diagrams in the frequency range of 0.01-1 MHz were used as a preliminary ER-EIS method adjustment. The sensitive nature of the experimental method requires the experiment to be conducted in an inert atmosphere, yielding reproducible measured DOS spectra.

Solid-State NMR: Spin-coated thin films of PTB7-Th and MEH-PPV were scratched off by using a scraper blade and the extracted powdered films were packed into 1.3 and 2.5 mm (outer diameter) zirconia rotors fitted with Vespel caps. Single-pulse ^{1}H MAS NMR spectra of PTB7-Th and MEH-PPV were acquired at 11.7 T, 298 K, and 58 kHz MAS on a Bruker AVANCE-II NMR spectrometer operating at a ^{1}H frequency of 500.2 MHz and equipped with Bruker 1.3 mm H-X MAS probehead; 32 co-added transients were signal-averaged using a recycle delay of 3 s, corresponding to a total experimental time of 2 min for each spectrum. 1D ^{19}F and ^{13}C MAS NMR spectra were acquired at 9.4 T and 298 K on a Bruker AVANCE-III NMR spectrometer operating at a ^{19}F frequency of 376.5 MHz and a ^{13}C frequency of 100.6 MHz equipped with a 2.5 mm H-F-X MAS probehead. A 1D single-pulse ^{19}F MAS spectrum of PTB7-Th was acquired at 30 kHz MAS with 512 co-added transients and a recycle delay of 15 s, corresponding to a total experimental time of 2 h. A 1D single-pulse ^{13}C MAS spectrum of MEH-PPV was acquired at 15 kHz MAS with 7568 co-added transients and recycle delay of 10 s, corresponding to a total experimental time of 21 h. Heteronuclear decoupling was applied during acquisition using the SPINAL64 pulse sequence.[71]

GIWAXS: GIWAXS measurements were performed at beamline 7.3.3 at the Advanced Light Source with an X-ray wavelength of 1.2398 A at a 300 mm sample detector distance. The measurements were calibrated using a AgB standard. Samples were scanned in a He environment at an incident angle of 0.14°.

References

[1] S. Günes, H. Neugebauer, N. S. Sariciftci, Chem. Rev. **2007**, 107, 1324.

[2] G. Horowitz, Adv. Mater. **1998**, 10, 365.

[3] K. M. Vaeth, Inf. Disp. **2003**, 19, 12.

[4] H. Bässler, Phys. Status Solidi (b) **1993**, 175, 15.

[5] J. C. Blakesley, D. Neher, Phys. Rev. B **2011**, 84, 075210.

[6] K. Celebi, P. J. Jadhav, K. M. Milaninia, M. Bora, M. A. Baldo, Appl. Phys. Lett. **2008**, 93, 083308.

[7] I. N. Hulea, H. B. Brom, A. J. Houtepen, D. Vanmaekelbergh, J. J. Kelly, E. A. Meulenkamp, Phys. Rev. Lett. **2004**, 93, 166601.

[8] O. Tal, Y. Rosenwaks, Y. Preezant, N. Tessler, C. K. Chan, A. Kahn, Phys. Rev. Lett. **2005**, 95, 256405.

[9] T. Sueyoshi, H. Fukagawa, M. Ono, S. Kera, N. Ueno, Appl. Phys. Lett. **2009**, 95, 183303.

[10] G. Garcia-Belmonte, P. P. Boix, J. Bisquert, M. Sessolo, H. J. Bolink, Sol. Energy Mater. Sol. Cells **2010**, 94, 366.

[11] M. Tachiya, K. Seki, Phys. Rev. B **2010**, 82, 085201.

[12] Z. M. Beiley, E. T. Hoke, R. Noriega, J. Dacuña, G. F. Burkhard, J. A. Bartelt, A. Salleo, M. F. Toney, M. D. McGehee, Adv. Energy Mater. **2011**, 1, 954.

[13] R. C. I. MacKenzie, T. Kirchartz, G. F. A. Dibb, J. Nelson, J. Phys. Chem. C **2011**, 115, 9806.

[14] W. Gong, M. A. Faist, N. J. Ekins-Daukes, Z. Xu, D. D. C. Bradley, J. Nelson, T. Kirchartz, Phys. Rev. B **2012**, 86, 024201.

[15] R. C. I. MacKenzie, C. G. Shuttle, M. L. Chabinyc, J. Nelson, Adv. Energy Mater. **2012**, 2, 662.

[16] C. G. Shuttle, N. D. Treat, J. D. Douglas, J. M. J. Fréchet, M. L. Chabinyc, Adv. Energy Mater. **2012**, 2, 111.

[17] J. O. Oelerich, D. Huemmer, S. D. Baranovskii, Phys. Rev. Lett. **2012**, 108, 226403.

[18] P. Pingel, D. Neher, Phys. Rev. B **2013**, 87, 115209.

[19] I. I. Fishchuk, A. K. Kadashchuk, J. Genoe, M. Ullah, H. Sitter, T. B. Singh, N. S. Sariciftci, H. Bässler, Phys. Rev. B **2010**, 81, 045202.

[20] F. Torricelli, Z. M. Kovács-Vajna, L. Colalongo, Org. Electron. **2009**, 10, 1037.

[21] M. Oehzelt, N. Koch, G. Heimel, Nat. Commun. **2014**, 5, 4174.

[22] N. I. Craciun, J. Wildeman, P. W. M. Blom, Phys. Rev. Lett. **2008**, 100, 056601.

[23] M. Kuik, G.-J. A. H. Wetzelaer, H. T. Nicolai, N. I. Craciun, D. M. D. Leeuw, P. W. M. Blom, Adv. Mater. **2014**, 26, 512.

[24] H. Yan, Z. Chen, Y. Zheng, C. Newman, J. R. Quinn, F. Dötz, M. Kastler, A. Facchetti, Nature **2009**, 457, 679.

[25] H.-R. Tseng, H. Phan, C. Luo, M. Wang, L. A. Perez, S. N. Patel, L. Ying, E. J. Kramer, T.-Q. Nguyen, G. C. Bazan, A. J. Heeger, Adv. Mater. **2014**, 26, 2993.

[26] H. Chen, Y. Guo, G. Yu, Y. Zhao, J. Zhang, D. Gao, H. Liu, Y. Liu, Adv. Mater. **2012**, 24, 4618.

[27] I. McCulloch, M. Heeney, C. Bailey, K. Genevicius, I. Macdonald, M. Shkunov, D. Sparrowe, S. Tierney, R. Wagner, W. Zhang, M. L. Chabinyc, R. J. Kline, M. D. McGehee, M. F. Toney, Nat. Mater. **2006**, 5, 328.

[28] C. M. Proctor, J. A. Love, T.-Q. Nguyen, Adv. Mater. **2014**, 26, 5957.

[29] C. M. Proctor, C. Kim, D. Neher, T.-Q. Nguyen, Adv. Funct. Mater. **2013**, 23, 3584.

[30] B. H. Hamadani, D. J. Gundlach, I. McCulloch, M. Heeney, Appl. Phys. Lett. **2007**, 91, 243512.

[31] M. L. Chabinyc, M. F. Toney, R. J. Kline, I. McCulloch, M. Heeney, J. Am. Chem. Soc. **2007**, 129, 3226.

[32] M. Kröger, S. Hamwi, J. Meyer, T. Riedl, W. Kowalsky, A. Kahn, Appl. Phys. Lett. **2009**, 95, 123301.

[33] G. A. H. Wetzelaer, P. W. M. Blom, Phys. Rev. B **2014**, 89, 241201.

[34] S.-H. Liao, H.-J. Jhuo, Y.-S. Cheng, S.-A. Chen, Adv. Mater. **2013**, 25, 4766.

[35] L. Pauling, J. Phys. Chem. **1941**, 45, 1142.

[36] P. W. M. Blom, M. J. M. de Jong, J. J. M. Vleggaar, Appl. Phys. Lett. **1996**, 68, 3308.

[37] C. Tanase, E. J. Meijer, P. W. M. Blom, D. M. de Leeuw, Phys. Rev. Lett. **2003**, 91, 216601.

[38] W. F. Pasveer, J. Cottaar, C. Tanase, R. Coehoorn, P. A. Bobbert, P. W. M. Blom, D. M. de Leeuw, M. A. J. Michels, Phys. Rev. Lett. **2005**, 94, 206601.

[39] L. J. A. Koster, E. C. P. Smits, V. D. Mihailetchi, P. W. M. Blom, Phys. Rev. B **2005**, 72, 085205.

[40] G. a. H. Wetzelaer, AIP Adv. **2018**, 8, 035320.

[41] K. Koynov, A. Bahtiar, T. Ahn, R. M. Cordeiro, H.-H. Hörhold, C. Bubeck, Macromolecules **2006**, 39, 8692.

[42] R. J. Kline, M. D. McGehee, E. N. Kadnikova, J. Liu, J. M. J. Fréchet, M. F. Toney, Macromolecules **2005**, 38, 3312.

[43] M. Nonnenmacher, M. P. O'Boyle, H. K. Wickramasinghe, Appl. Phys. Lett. **1991**, 58, 2921.

[44] L. Kelvin, Lond. Edinb. Dublin Philos. Mag. J. Sci. **1898**, 46, 82.

[45] J. C. Blakesley, N. C. Greenham, J. Appl. Phys. **2009**, 106, 034507.

[46] I. Lange, J. C. Blakesley, J. Frisch, A. Vollmer, N. Koch, D. Neher, Phys. Rev. Lett. **2011**, 106, 216402.

[47] O. M. Ottinger, C. Melzer, H. von Seggern, J. Appl. Phys. **2009**, 106, 023704.

[48] A. Köhler, H. Bässler, Electronic Processes in Organic Semiconductors, 1st ed., Wiley-VCH, Weinheim, Germany **2015**.

[49] S. D. Collins, C. M. Proctor, N. A. Ran, T.-Q. Nguyen, Adv. Energy Mater. **2016**, 6, 1501721.

[50] N. A. Ran, J. A. Love, C. J. Takacs, A. Sadhanala, J. K. Beavers, S. D. Collins, Y. Huang, M. Wang, R. H. Friend, G. C. Bazan, T.-Q. Nguyen, Adv. Mater. **2016**, 28, 1482.

[51] R. A. Marcus, J. Chem. Phys. **1956**, 24, 966.

[52] F. Schauer, V. Nádaždy, K. Gmucová, J. Appl. Phys. **2018**, 123, 161590.

[53] V. Nádaždy, F. Schauer, K. Gmucová, Appl. Phys. Lett. **2014**, 105, 142109.

[54] G. Garcia-Belmonte, J. Bisquert, G. S. Popkirov, Appl. Phys. Lett. **2003**, 83, 2178.

[55] J. Bisquert, G. Garcia-Belmonte, J. García-Cañadas, J. Chem. Phys. **2004**, 120, 6726.

[56] Z. Pomerantz, A. Zaban, S. Ghosh, J.-P. Lellouche, G. Garcia-Belmonte, J. Bisquert, J. Electroanal. Chem. **2008**, 614, 49.

[57] V. Coropceanu, J. Cornil, D. A. da Silva Filho, Y. Olivier, R. Silbey, J.-L. Brédas, Chem. Rev. **2007**, 107, 926.

[58] R. Noriega, J. Rivnay, K. Vandewal, F. P. V. Koch, N. Stingelin, P. Smith, M. F. Toney, A. Salleo, Nat. Mater. **2013**, 12, 1038.

[59] H. Sirringhaus, P. J. Brown, R. H. Friend, M. M. Nielsen, K. Bechgaard, B. M. W. Langeveld-Voss, A. J. H. Spiering, R. a. J. Janssen, E. W. Meijer, P. Herwig, D. M. de Leeuw, Nature **1999**, 401, 685.

[60] J. Rivnay, S. C. B. Mannsfeld, C. E. Miller, A. Salleo, M. F. Toney, Chem. Rev. 2012, 112, 5488.

[61] H. W. Ro, J. M. Downing, S. Engmann, A. A. Herzing, D. M. DeLongchamp, L. J. Richter, S. Mukherjee, H. Ade, M. Abdelsamie, L. K. Jagadamma, A. Amassian, Y. Liu, H. Yan, Energy Environ. Sci. **2016**, 9, 2835.

[62] G. N. M. Reddy, A. Huqi, D. Iuga, S. Sakurai, A. Marsh, J. T. Davis, S. Masiero, S. P. Brown, Chem. Eur. J. **2017**, 23, 2315.

[63] M. R. Hansen, R. Graf, H. W. Spiess, Chem. Rev. **2016**, 116, 1272.

[64] A. Melnyk, M. J. N. Junk, M. D. McGehee, B. F. Chmelka, M. R. Hansen, D. Andrienko, J. Phys. Chem. Lett. **2017**, 8, 4155.

[65] C. K. Lo, B. R. Gautam, P. Selter, Z. Zheng, S. D. Oosterhout, I. Constantinou, R. Knitsch, R. M. W. Wolfe, X. Yi, J.-L. Brédas, F. So, M. F. Toney, V. Coropceanu, M. R. Hansen, K. Gundogdu, J. R. Reynolds, Chem. Mater. **2018**, 30, 2995.

[66] F. Kraffert, D. Bahro, C. Meier, M. Denne, A. Colsmann, J. Behrends, J. Magn. Reson. **2017**, 282, 10.

[67] C. Jing, L. Chen, Y. Shi, X. Jin, Eur. Polym. J. **2005**, 41, 2388.

[68] M. J. N. Junk, G. N. M. Reddy, D. Dudenko, A. Melnyk, N. C. Miller, S. Sweetnam, M. D. McGehee, D. Andrienko, M. R. Hansen, B. F. Chmelka, **2019**, unpublished.

[69] X. Cui, M. Freitag, R. Martel, L. Brus, P. Avouris, Nano Lett. **2003**, 3, 783.

[70] S. Suzuki, C. Bower, Y. Watanabe, O. Zhou, Appl. Phys. Lett. **2000**, 76, 4007.

[71] B. M. Fung, A. K. Khitrin, K. Ermolaev, J. Magn. Reson. San Diego Calif 1997 **2000**, 142, 97.